Lowland Technology International 2018; 19 (4): 237-244
International Association of Lowland Technology (IALT): ISSN 1344-9656
Special Issue on: Kumamoto Earthquake & Disaster

Research Paper

Deformation and failure characteristics of Volcanic soil at landslides site due to the 2016 Kumamoto Earthquake

W. O. Sumartini [1], H. Hazarika [2], T. Kokusho [3], S. Ishibashi [4], D. Matsumoto [5] and B. Chaudhary [6]

ARTICLE INFORMATION

Article history:

Received: 06 March, 2017
Received in revised form: 21 February, 2018
Accepted: 23 February, 2018
Publish on: 09 March, 2018

Keywords:

Volcanic soil
The 2016 Kumamoto Earthquake
Static triaxial test
Cyclic triaxial test
Mineralogy
Soil fabric

ABSTRACT

A chain of earthquakes with a maximum moment magnitude of 7.3 MW struck Kumamoto prefecture and its vicinity from April 14-16th, 2016. It generated widespread landslides not only on steep slopes but also on gentle slopes. The landslides caused huge damages to nature, infrastructure, and loss of lives. Thus, it is crucial to determine the failure mechanism of those slopes which were formed by volcanic soil and to elucidate the effect of cyclic loading on strength characteristics of the soil. A series of investigations of the soil, which is orange colored, was conducted. Undrained static and cyclic triaxial tests were performed. Also, x-ray powder diffraction test, x-ray fluorescence test, and scanning electron microscope test were performed for further understanding of the material behavior. The triaxial test revealed semi dilative behavior under monotonic loading with small confining stress and contractive behavior on high confining stress. In the cyclic triaxial tests under in situ confining stress, cyclic mobility by lower cyclic stress and flow failure by higher cyclic stress was observed. Also, soil fabric, chemical composition, and mineral composition, which describe the deformation behavior and failure characteristics of the soil has been reported.

1. Introduction

Volcanic soil is known for being problematic and hazardous with its peculiar behavior. It is ejected from volcanic activity and has unique properties in its mineral content, chemical content, porosity, fabric, interlocking between grains and cementation process.

In Japan, significant geotechnical damages occurred in volcanic soil areas due to earthquakes (Hazarika et al., 2018; Kayen et al., 2016; Miyagi et al., 2011; Kazama et al., 2012; Sassa, 2005). From 14th to 16th April 2016, a chain of earthquakes occurred in Kumamoto prefecture, Japan. It was a series of earthquakes, including a magnitude 6.5 MW foreshock and 7.0 MW main shock called the 2016 Kumamoto Earthquake. These chain of events demonstrated the impact of the earthquake on infrastructures, houses (**Fig. 1**), bridges (**Fig. 2**), roads (**Fig. 3**), and other engineering properties and even loss of lives. During the earthquake, seismic subsidences, widespread landslides, slope failures, debris flows, and liquefactions were observed in Kumamoto prefecture and its vicinity. The landslides occurred on steep as well as

[1] PhD Student, Department of Civil Engineering, Kyushu University, Fukuoka, JAPAN, waode_sumartini@yahoo.co.id
[2] Professor, Department of Civil Engineering, Kyushu University, Fukuoka, JAPAN, hazarika@civil.kyushu-u.ac.jp
[3] Professor Emeritus, Chuo University, Tokyo, JAPAN, koktak@ad.email.ne.jp
[4] Assistant Manager, Survey and Analysis Department, Nihon Chiken Co., Ltd., Fukuoka, JAPAN, Ishibashi@chiken.co.jp
[5] Manager, Japan Foundation Engineering Co., Ltd., Fukuoka, JAPAN, daisuke_matsumoto@jafec.co.jp
[6] Postdoctoral Fellow, Division of Environmental Science and Technology, Kyoto University, Kyoto, JAPAN, babloomit@gmail.com
Note: Discussion on this paper is open until September 2018.

Fig. 1. Houses damages due to subsidence.

Fig. 2. Bridge collapse and landslide.

Fig. 3. Damages to road.

on gentle slopes even though landslides rarely occurred on gentle slopes. One of the landslides is located close to Aso Volcanological Laboratory of Kyoto University as shown in **Fig. 4**. The slope has a gentle inclination (10 to 15 degrees) as reported by Kochi et al. (2017). It has many volcanic soil deposits with distinct colors. All of the deposits were failed other than the deposits below Orange colored deposits. They scattered in big and small lumps except the Orange colored deposit which crumbled as shown in **Fig. 5**. Therefore, the authors suspect that

Fig. 4. Location of sampling sites, Aso Caldera, Kumamoto Prefecture, Japan.

Fig. 5. Volcanic soil deposits after landslide.

the landslide occurred due to liquefaction of the Orange colored deposits.

A simplified methodology to evaluate lateral deformation and settlement of residence construction on volcanic ash cohesive soils induced by the earthquake was reported by Yasuhara et al. (2017). However, the deformation and failure characteristics of the soil deposit related to the landslide induced by the earthquake have not been done. Thus, the authors investigated this phenomenon and elucidated the soil characteristics. They were investigated by a series of undrained static and cyclic triaxial tests. Triaxial test is a common method that has been used to define the liquefaction susceptibility and strength characteristics of volcanic soils (Ishikawa et al., 2011; Suzuki and Yamamoto, 2004; Hatanaka et al., 1985). Also, for further understanding of the soil material strength, X-ray powder diffraction analysis (XRD), X-ray fluorescence analysis (XRF), and Scanning electron microscope analysis (SEM) were performed. In this paper, preliminary results of these tests are discussed.

2. Geological aspects

The cliff of Aso caldera has numerous soil layer deposits, which originated from volcanic ejections from several volcano activities on Kyushu Island. The cliff in the study area has different colors and characteristics which have been drawn by Sumartini et al. (2017) in **Fig. 6**. They identified seven different volcanic layers in the volcaniclastic sequence of the cliff. Kochi et al. (2017) reported that each layer of the cliff originated from different places and ages as listed in **Table 1**. Orange soil, which originated from Kusasenrigahama Pumice (Kpfa) along with other deposits above it, were considered younger than Pre Takanoobane lava pumice deposits.

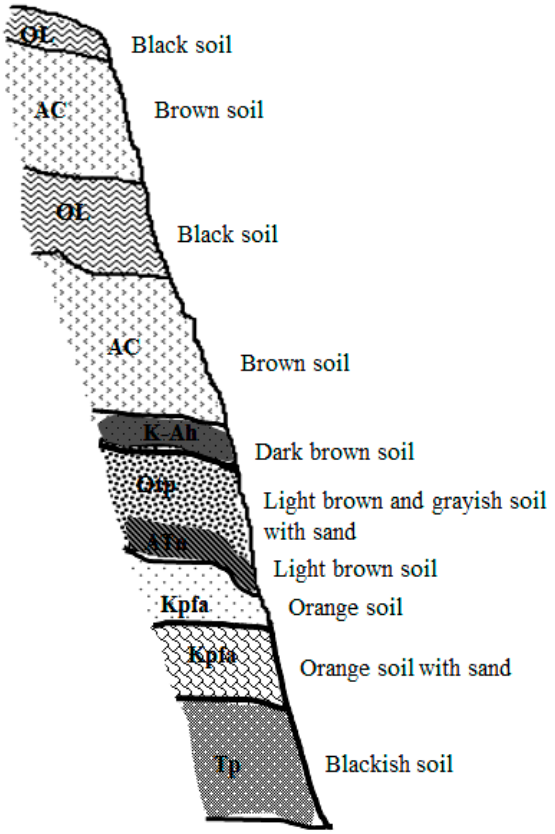

Fig. 6. The schematic profile and physical description of cliff with volcanic soil deposits (Sumartini et al., 2017).

Table 1. Origin of volcanic soil in Aso Caldera (Kochi et al., 2017).

Origin		Age
Organic, OL	(cal ka)	10-present
Aso Central Cone Pumice, AC	(cal ka)	7.3-10
Kikai Akahoya Ash, K-Ah	(cal ka)	7.3
Otogase Lava Pumice, Otp	(cal ka)	29-7.3
Aira Tn, Atn	(cal ka)	29
Kusasenrigahama Pumice, Kpfa	(cal ka)	31
Pre Takanoobane Lava Pumice, Tp	(cal ka)	51±5

3. Soil sampling

The soil was collected using steel tube samplers as shown in **Fig. 7**, at a ground depth of 5 m at the scarp in landslide sites near the Kyoto University Volcano Research Center, as shown in **Fig. 4**. The collected samples were then assumed to be undisturbed even though some disturbing effects were suspected during the collecting process despite no visible damage by the process. After the undisturbed samples were tested, they were reconstituted and then tested as disturbed samples. In order to differentiate them from other volcanic soils in the Aso area, the soil samples were named as Orange soil in this research.

Fig. 7. Collecting volcanic soil using steel tube sampler.

Table 2. Physical properties of Orange soil.

Physical properties		Orange soil
Specific gravity		2.24-2.38
Dry density, ρ_d	(g/cm^3)	0.51-0.58
Wet density, ρ_t	(g/cm^3)	1.23-1.30
Water content, w	(%)	54.62-58.36
Liquid limit, w_L	(%)	113.40
Plastic limit, w_P	(%)	88.25
Plasticity index, I_p		25.15

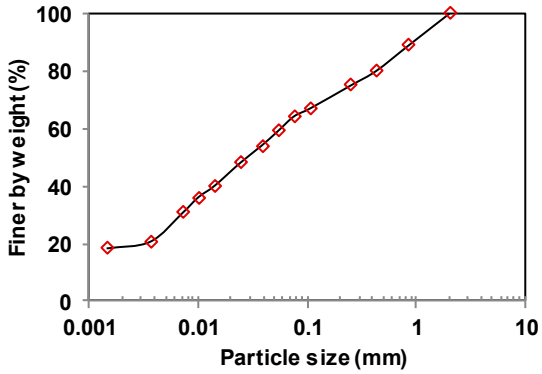

Fig. 8. Grain size distribution of Orange soil.

Physical properties of the Orange soil are listed in **Table 2**. It shows that the specific gravity of the Orange soil ranges from 2.24 to 2.38, which considered low compared to ordinary silt. The Orange soil also has a high plasticity index and has low dry density. The grain size distribution is shown in **Fig. 8**. It reveals that the Orange soil contains 35.8 % of sand, 39.2 % of silt and 25.0 % of clay. Based on its properties and grain size distribution by JGS soil classification, Orange soil is classified as volcanic cohesive soil type II (VH_2).

4. Evaluation process

The deformation and strength characteristics of Orange soil were evaluated by static and cyclic triaxial tests in undrained condition, as well as XRD, XRF, and SEM analysis. In the triaxial tests, double negative pressure and appropriate back pressure were applied to the samples and they were isotropically consolidated at the target effective pressure. B-values > 0.95 were ensured for all samples before shearing. The samples were 50 mm in diameter and 100 mm in height. For triaxial static test, strain control was applied up to 20 % and the shearing speed was 0.1 % strain per minute. The frequency of the axial load was 0.1 Hz for the undrained triaxial cyclic tests. On the other hand, dried samples were used in XRD, XRF, and SEM analysis. The samples were prepared under air-dried conditions to maintain the natural condition and avoid changes in mineral and chemical composition due to high temperature.

5. Results and discussion

5.1 Soil behavior under static loading

The **Figures 9** and **10** show the results of the undrained static triaxial test of the Orange soil of undisturbed and disturbed samples respectively. Comparing the stress versus strain of disturbed samples (**Fig. 9a**) and disturbed samples (**Fig. 10a**), the undisturbed samples exhibited a significantly different stress-strain response with much higher stresses. However, the development of the pore water pressure of both samples is not so much different as shown in **Figures 9b** and **10b**. Under low confining stress, the peak stress of undisturbed samples is about three times higher than disturbed samples. Meanwhile, the strain is about three to four times lower than disturbed samples. On the other hand, under high confining pressure, the peak stress of disturbed samples is about ¾ times that of undisturbed samples and the strain is similar.

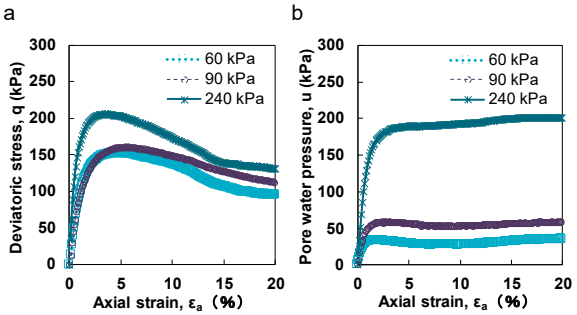

Fig. 9. Response of the undisturbed Orange soil samples in undrained static triaxial test: (a) Stress versus axial strain and (b) Pore water pressure versus axial strain.

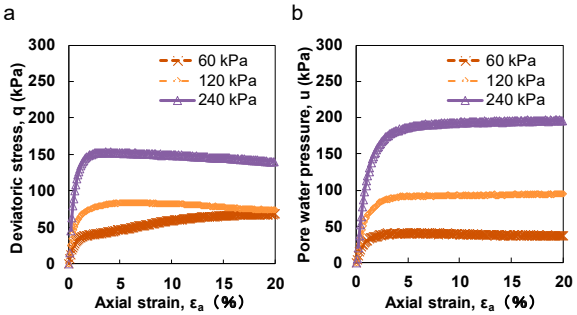

Fig. 10. Response of the disturbed Orange soil samples in undrained static triaxial test: (a) Stress versus axial strain and (b) Pore water pressure versus axial strain.

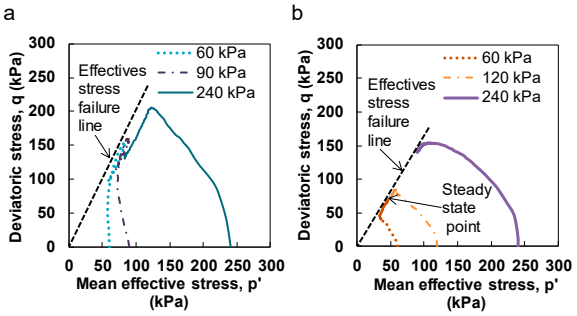

Fig. 11. Stress path of the Orange soil: (a) Undisturbed and (b) Disturbed samples.

Figure 11 displays the stress path of the undisturbed and the disturbed samples. The undisturbed samples (**Fig. 11a**) show dilative behavior up to the failure line under an initial effective confining stress of 60 kPa and 90 kPa, though it is followed by sudden contractive failure presumably due to particle breakage of weak pumice grains at their contacts. The disturbed samples (**Fig. 11b**) show contractive behavior under 120 kPa, and 240 kPa initial effective confining pressures versus dilative behavior under 60 kPa wherein no sudden contractive failure appears. A similar contractive behavior occurs only under 240 kPa for the undisturbed samples.

5.2 Soil behavior under cyclic loading

Figures 12, 13, 14, and 15 present the response of Orange soil in undrained cyclic triaxial tests all conducted under an effective confining stress 60 kPa which is roughly equal to in situ stress for the Orange soil. The undisturbed samples under CSR = 0.274, 0.426 and 0.502 show cyclic mobility behavior and moderate cyclic shear strain. This possibly occurred because of the plasticity index (**Table 2**) and the fines content (**Fig. 8**) of the Orange soil are high. In addition, correlating with the static test results as shown in **Fig. 10a**, it shows that the double amplitude of the shear stress of the samples were lower than the maximum deviatoric stress. The samples

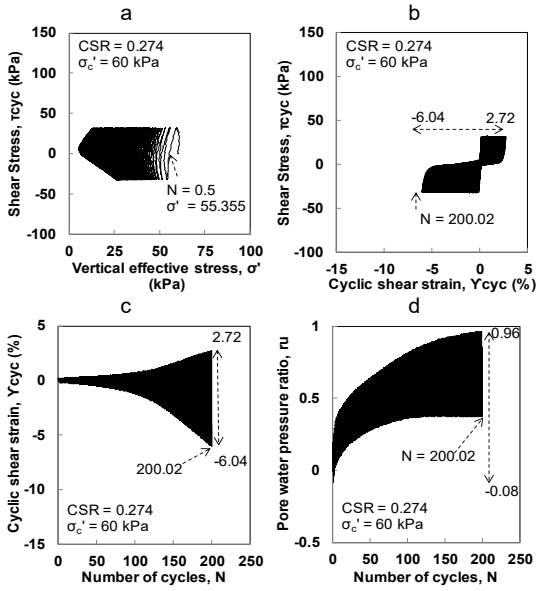

Fig. 12. Response of the undisturbed Orange soil samples in undrained cyclic triaxial test (CSR = 0.274, σ_c' = 60 kPa): (a) effective stress path, (b) shear stress versus shear strain, (c) shear strain versus number of cycles, and (d) pore water pressure ratio versus number of cycles.

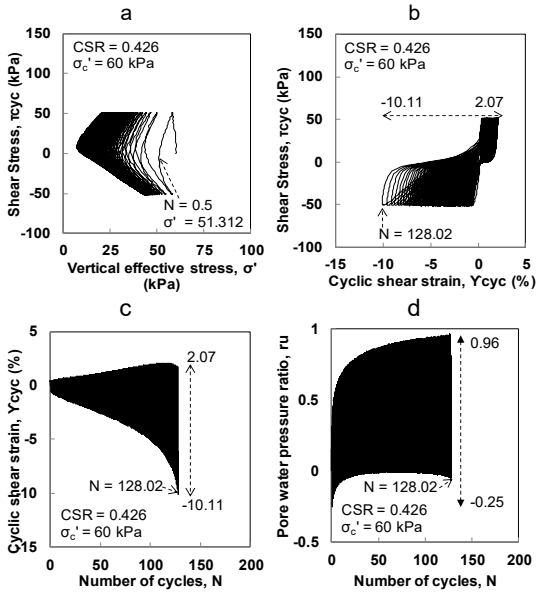

Fig. 13. Response of the undisturbed Orange soil samples in undrained cyclic triaxial test (CSR = 0.426, σ_c' = 60 kPa): (a) effective stress path, (b) shear stress versus shear strain, (c) shear strain versus number of cycles, and (d) pore water pressure ratio versus number of cycles.

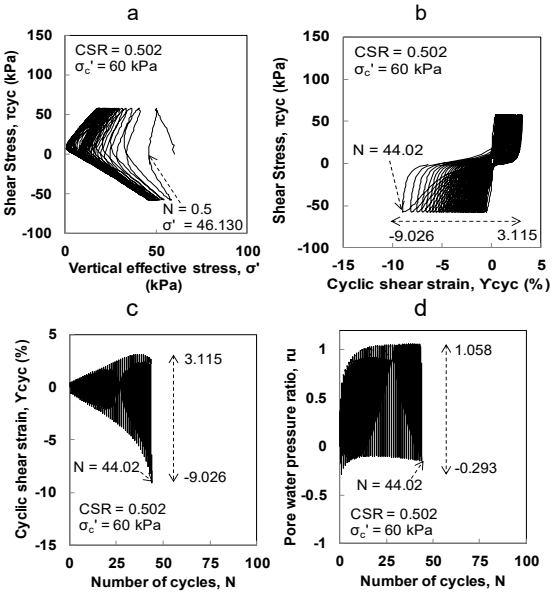

Fig. 14. Response of the undisturbed Orange soil samples in undrained cyclic triaxial test (CSR = 0.502, σ_c' = 60 kPa): (a) effective stress path, (b) shear stress versus shear strain, (c) shear strain versus number of cycles, and (d) pore water pressure ratio versus number of cycles.

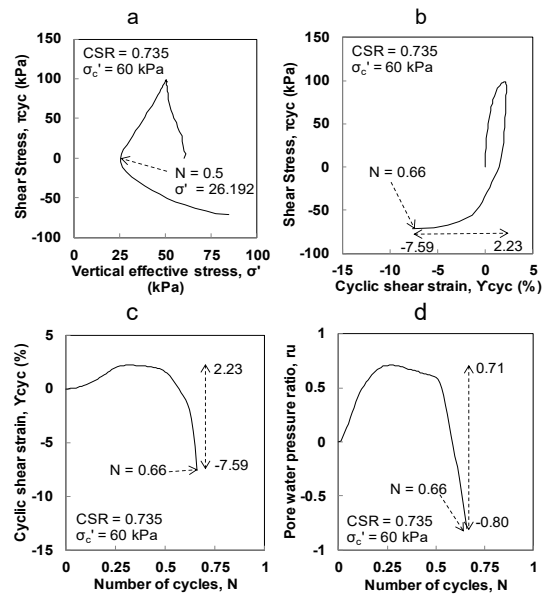

Fig. 15. Response of the undisturbed Orange soil samples in undrained cyclic triaxial test (CSR = 0.735, σ_c' = 60 kPa): (a) effective stress path, (b) shear stress versus shear strain, (c) shear strain versus number of cycles, and (d) pore water pressure ratio versus number of cycles.

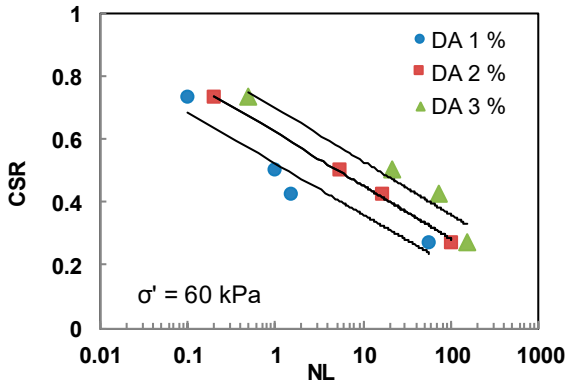

Fig. 16. Liquefaction susceptibility of Orange soil.

0.274 and 0.426 of CSR display similar stress-strain behavior with sample 0.502 of CSR, otherwise they did not reach a similar peak on pore water pressure ratio. Their pore water pressure ratio is not more than 0.96 while that of the sample 0.502 of CSR is 1.058. This probably occurred due to the fact that their shear stress amplitude is lower than the confining pressure.

The undisturbed sample under CSR = 0.735 shows the flow type failure behavior, pore water pressure ratio = 0.713, and fast development of cyclic shear strain. This occurred due to the shear stress amplitude being greater than half of the maximum deviatoric stress of the soil. The investigated samples exhibit cyclic mobility behaviours except that with CSR = 0.735, revealing that the undisturbed samples were less susceptible to flow type failure in cyclic loading under the confining stress 60 kPa except if the double shear stress amplitude exceeds the maximum deviatoric stress.

To cause a 5% double amplitude axial strain of Orange soil in 20 cycles, cyclic stress ratio of 0.50 was required as shown in **Fig. 16**. This occurred because the plasticity index of the soil is high, as shown in Table 2 and the shear strength being 2.5 times higher than the confining stress means that the soil is strong enough to bear the cyclic load even though the shear stress amplitude equals the confining stress.

5.3 Soil mineral content

The XRD analysis results show that the Orange soil contains 57% high mineral Albite and 40% mineral Bytownite, as shown in **Table 3**. These two minerals are members of Plagioclase feldspar (Galleries) group. In other words, the Orange soil contains 97 % of Feldspar. Feldspar is the principal aluminum-bearing mineral in the parent rock and is completely destroyed during weathering (Patterson, 1971). Consequently, it can be assumed that the Orange soil contains high aluminum and its minerals has been destroyed during weathering.

Table 3. Mineralogical content of Orange soil.

Mineralogical content	(%)
Albite	57
Bytownite	40
Sodium hydrogen sulfide	2.0
Calsium copper germanium oxide	1.4

5.4 Soil chemical content

Table 4 presents the chemical composition of the XRF analysis. The Orange soil contains 3.628 % of alkaline metal and alkaline metal earths which is considered low. This indicates that the soil has been weathered for a long time since the alkalies and the alkaline earths are removed during weathering along with soil hardness (Patterson, 1971). In other words, it explains that the Orange soil has brittle tenacity. Al_2O_3 concentration is 35.959 %, which is the second dominant content after SiO_2. This correlates to the XRD results that the Orange soil contains Feldspar which is the principal aluminum bearing mineral. Considering the alkalies and alkaline earths concentration, alumina is typically high from Al replacing SiO_2 during the weathering (Patterson, 1971). The high concentration of alumina also indicates the occurrence of nodules meanwhile Al is conveyed in the weathered deposits by groundwater even though much of Al is a residual concentration (Patterson, 1971).

5.5 Effect of cyclic loading on soil fabric

The SEM analysis results of the Orange soil fabric before and after cyclic loading test is displayed in **Figures 17** and **18** respectively. As seen from **Fig. 17**, the soil skeleton is formed by crystal flakes with high porosity. By comparing it to **Fig. 18**, the skeleton of the soil was visibly broken and the crystal flakes sizes reduced. Thus, it can be deduced that the quantity of fine particle is increased after cyclic loading due to the breakage of the soil skeleton.

Table 4. Chemical content of Orange soil.

Chemical content	(%)
SiO_2	48.832
Al_2O_3	35.959
Fe_2O_3	8.910
CaO	3.300
TiO_2	1.843
P_2O_5	0.489
K_2O	0.259
MnO	0.172
SrO	0.069
ZrO_2	0.065
SO_3	0.060
Ag_2O	0.018
Y_2O_3	0.008
ZnO	0.008
Ga_2O_3	0.007
NbO	0.003

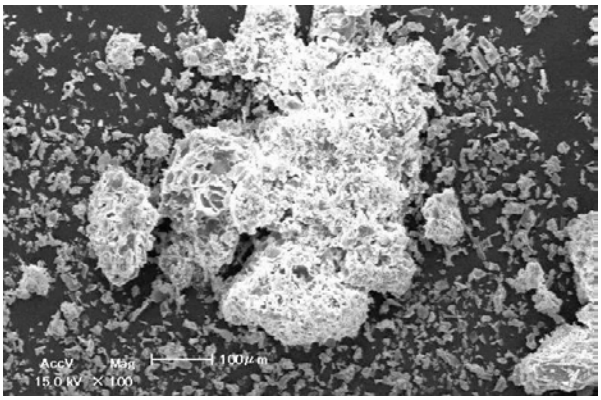

Fig. 17. Orange soil fabric before cyclic loading.

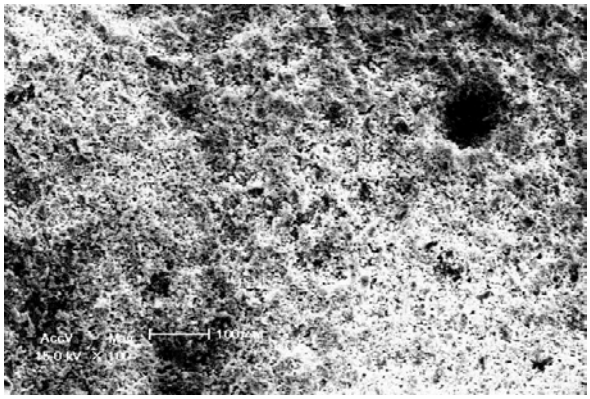

Fig. 18. Orange soil fabric after cyclic loading.

6. Conclusions

Based on this comprehensive investigation, the following conclusions are derived:

1. The peak strength of the disturbed samples was significantly lower than that for the undisturbed samples. The significant difference in stress-strain behavior and shear strength between the undisturbed and disturbed samples was caused by changes in the soil microstructure.
2. Considering the dramatic change of the Orange soil behavior under static loading, it is strongly recommended not to use the disturbed samples results as they may give a wrong impression on deformation and stability analyses. On the other hand, it is difficult to collect the Orange soil in an undisturbed condition due to its brittleness. Consequently, it is highly suggested to develop a treatment method on the disturbed soil which can match the behavior of the undisturbed samples.
3. The cyclic test revealed that the Orange soil is liquefied when the cyclic stress is greater than the confining pressure. It means that the Orange soil has low liquefaction susceptibility.
4. Correlating the results of the static and the cyclic tests shows that the cyclic mobility occurred when DA of $\tau_{cyc}<q_{max}$ and the flow type failure occurred when DA of $\tau_{cyc}>q_{max}$. It can be deduced that the stress-strain curve of the static test can be used in predicting the required CSR of the flow type failure.
5. Although the plasticity index and the fine content of the Orange soil are high, liquefaction occurred in the investigated samples. This confirms that the Orange soil deposits were liquefying during the earthquake which caused the landslide. However, in order to obtain an accurate explanation of the Orange soil behavior during the earthquake, investigation under a similar frequency as the earthquake is strongly recommended.
6. XRD, XRF, and SEM tests revealed that the Orange soil has brittle mineralogy, lack of alkaline metal and alkaline metal earths, and a high porosity, which describes the deformation behavior of the Orange soil.

Acknowledgments

The financial grant for this research under the J-RAPID program (Principal Investigator: Hemanta Hazarika) of Japan Science and Technology Agency (JST) is gratefully acknowledged.

The authors are grateful to Mr. Katsuki Yoshinori (Nihon Chiken Co., Ltd.) for providing laboratory for this research and Dr. Watanabe Midori (Kyushu University) for her guidance in SEM, XRF and XRD tests. The first author also wishes to express her sincere thanks to Mr. Ogo Katsuya (Kyushu University), Mr. Siavash Manafi Khajeh Pasha (Kyushu University), Mrs. Sito Ismanti (Kyushu University) and Mr. Jalalya Mabojano (Kyushu University) for their helpful discussion related to triaxial testing. Mr. Feby Pratama (Kyushu University), Ms. Intan Nurul Rizki (Kyushu University), Ms. Tran Thi Thanh *Thuy* (Gadjah Mada University) and Ms. Fadiah Pratiwi (Kyushu University) are gratefully acknowledged for their kind information related to the preparation of samples and interpretation results of XRD and XRF tests. First author's great appreciations also go to Ms. Hajrah (Stuttgart University, Germany) for her valuable information related to this research. Last but not the least, the first author is also grateful to the Indonesia Endowment Fund for Education (LPDP) for financially supporting her study.

References

Galleries. The Feldspar Group. Amethyst Galleries, Inc. http://www.galleries.com/Feldspar_Group, 2018.

Hatanaka, M., Sugimoto, M. and Suzuki, Y., 1985. Liquefaction resistance of two alluvial volcanic soils sampled by in situ freezing. Soils and Foundations, **25** (3): 49-63.

Hazarika, H., Kokusho, T., Kayen, R.E., Dashti, S., Fukuoka, H., Ishizawa, T., Kochi, Y., Matsumoto, D., Hirose, T., Furuichi, H., Fujishiro, T., Okamoto, K., Tajiri, M. and Fukuda, M., 2017. Geotechnical damage due to the 2016 Kumamoto Earthquake and future challenges. Lowland Technology International, Special Issue on the 2016 Kumamoto Earthquake and Geodisasters, **19** (3): 189-204.

Ishikawa, T. and Miura, S., 2011. Influence of freeze-thaw action on deformation-strength characteristics and particle crushability of volcanic coarse-grained soils. Soils and Foundations, **51** (5): 785 -799.

Kayen, R., Dashti, S., Kokusho, T., Hazarika, H., Franke, K., Oettle, N., Wham, B., Calderon, J.R., Briggs, D., Guillies, S., Cheng, K., Tanoue, Y., Takematsu, K., Matsumoto, D., Morinaga, T., Furuichi, H., Kitano, Y., Tajiri, M., Chaudhary, B., Nishimura, K. and Chu, C., 2016. Geotechnical aspects of the 2016 MW 6.2, MW 6.0, and MW 7.0 Kumamoto Earthquakes. GEER Report, University of Berkeley.

Kazama, M., Kataoka, S. and Uzuoka, R., 2012. Volcanic mountain area disaster caused by the Iwate-Miyagi Nairiku Earthquake of 2008. Soil and Foundations, **52** (1): 168-184.

Kochi, Y., Kariya, T., Kochi, Y., Matsumoto, D. and Hirose, T., 2017. Investigation of slopes on the Takanoobane Lava Dome using resistivity imaging method. Proc. International Workshop on the 2016 Kumamoto Earthquake, March 9, 2017, Kyushu Univ., Fukuoka, Japan: 95-100.

Miyagi, T., Higaki, D., Yagi, H., Yoshida, S., Chiba, N., Umemura, J. and Satoh, G., 2011. Reconnaissance report on landslide disaster in Northeast following the M 9 Tohoku Earthquake. Landslides, **8** (3): 339-342.

Patterson, S. H., 1971. Investigations of Ferruginous Bauxite and other mineral resources on Kauai and a reconnaissance of Ferruginous Bauxite Deposits on Maui, Hawaii. U.S. Geol. Survey Professional Paper 656, 74p.

Sassa, K., 2005. Landslide disasters triggered by the 2004 Mid-Niigata Prefecture earthquake in Japan. Landslides, **2** (2): 135-142.

Suzuki, M. and Yamamoto, T., 2004. Liquefaction characteristic of undisturbed volcanic soil in cyclic triaxial test. Proc. World Conference on Earthquake Engineering (13WCEE), August 1-6, 2004, Vancouver, B. C, Canada: Paper No. 465.

Sumartini, W. O., Hazarika, H., Kokusho, T., Ishibashi, S., Matsumoto, D. and Chaudhary, B., 2017. Liquefaction susceptibility of volcanic soil in Aso caldera due to the 2016 Kumamoto Earthquake. Proc. 19th International Summer Symposium, September 11-12, 2017, JSCE., Fukuoka, Japan: 13-14.

Yasuhara, K., Kobayashi, K., Watanabe, M., Yoshimi, M., Hosoya, T., Arai, Y. and Murakami, S., 2017. Instability of residences on volcanic ash cohesive soils during the 2016 Kumamoto Earthquake. International Workshop on the 2016 Kumamoto Earthquake, March 9, 2017, Kyushu Univ., Fukuoka, Japan: 139-146.

Symbols and abbreviations

AC	Aso Central Cone Pumice
Atn	Aira tn
CSR	Cyclic stress ratio
DA	Double amplitude
K-Ah	Kikai Akahoya
Kpfa	Kusasenrigahama Pumice
N	Number of cycles
NL	Number of cycles at liquefaction
OL	Organic
Otp	Otogase Lava Pumice
p’	Mean effective principal stress
q	Deviator stress
ru	Pore water pressure ratio
SEM	Scanning electron microscope
Tp	Pre Takanoobane Lava Pumice
u	pore water pressure
XRD	X-ray diffraction
XRF	X-ray fluorescence
γ_c	Cyclic shear strain
ε_a	Axial strain
σ_c'	Effective confining stress
σ'	Vertical Effective stress
τ_{cyc}	Cyclic shear stress